Construction and Building Materials 140 (2017) 100–108

Contents lists available at ScienceDirect

Construction and Building Materials

journal homepage: www.elsevier.com/locate/conbuildmat

Validation of a FEA model of structural response of RC-cantilever beams strengthened with a (R-) UHPFRC layer

Hamid Sadouki *, Emmanuel Denarié, Eugen Brühwiler

Maintenance and Safety of Structures, Ecole Polytechnique Fédérale de Lausanne (EPFL), CH-1015 Lausanne, Switzerland

HIGHLIGHTS

- Strengthening RC cantilever beam with a thin layer of UHPFRC increases considerably the bending resistance.
- FE model is elaborated for simulating structural behaviour of composite beams.
- The FE model reproduces accurately experimental force-deflection response.

ARTICLE INFO

Article history:
Received 12 September 2016
Received in revised form 15 February 2017
Accepted 18 February 2017

Keywords:
UHPFRC
Strengthening
Retrofitting
Composite cantilever beam
Nonlinear finite element modelling
Strain hardening
Strain softening

ABSTRACT

This paper focuses on modelling of structural response of RC cantilever beams retrofitted with a thin layer of Ultra High Performance Fibre Reinforced cement-based Composite (UHPFRC). The complex cracking phenomenon of the resulting RC-UHPFRC composite system is carried out by a numerical model incorporating the real nonlinear materials laws, in order to predict accurately the mechanical behaviour. To validate the model, experimental data obtained from RC-UHPFRC cantilever are confronted with the numerical findings. The model can predict efficiently the structural resistance of the tested composite systems. The model can be used for prediction purposes in design for real concrete structures strengthened by UHPFRC.

1. Introduction

In order to increase the resistance and service duration of existing reinforced concrete structures while ensuring structural safety and serviceability, a vast experimental campaign has been carried out for several years at our institute [1–6] to investigate the structural behaviour of reinforced concrete structural members strengthened by means of a layer of Ultra High Performance Fibre Reinforced cement-based Composite (UHPFRC) material. UHPFRC is a cement-based fibre reinforced composite material with high density due to optimized compaction of particles and a large percentage (more than 3% in volume) of short and slender steel fibres [4,7,8].

The use of UHPFRC for strengthening RC structures is motivated (1) by its outstanding mechanical properties, namely high tensile and compressive strengths and its important deformation capacity due to the high amount of incorporated steel fibres in the cement-based matrix of the material, and (2) by its very low porosity implying minimized moisture exchange and practically no ingress of chemical substances such as chloride ions from the surrounding atmosphere, consequently protecting steel reinforcement bars against corrosion [4]. In addition to its use for rehabilitation and strengthening of damaged existing RC structures, UHPFRC can also be used to replace conventional concrete of structural members of new structures exposed to severe environmental conditions and mechanical loading.

Fig. 1 shows stress-strain diagrams of 4 UHPFRC dog-bone specimens with a length of 350 mm subjected to uniaxial tension [5]. As illustrated in Fig. 1, UHPFRC behaviour in tension exhibits three phases: an elastic domain, followed by a stress-strain-hardening phase, characterized by multiple fine microcracks, invisible and quasi-homogenously distributed in the entire volume of the bulk material until the tensile strength is reached, and finally, beyond the tensile strength, a stress-strain-softening regime takes place;

* Corresponding author.
E-mail addresses: hamid.sadouki@epfl.ch (H. Sadouki), emmanuel.denarie@epfl.ch (E. Denarié), eugen.bruehwiler@epfl.ch (E. Brühwiler).

http://dx.doi.org/10.1016/j.conbuildmat.2017.02.090
0950-0618/

List of symbols

DB	dog-bone	f	strength
C	concrete	u	hardening
U	UHPFRC	1,2	index of connection points of the piecewise linear softening-diagrams
E	modulus of elasticity		
W	crack opening	σ	stress
F	force	ε	deformation
a, l	geometrical parameters of the cantilever beams	v	Poisson's ratio
c	compression	Φ,ϕ	diameter of steel rebars
e	elastic		
s	softening		
t	tensile		

this last phase is characterized by localization of deformations at an individual discrete macrocrack.

Experimental curves depicted in Fig. 1 show a relatively important scatter between the behaviour of the four specimens. The thick black curve in the figure represents the mean value of DB1 to DB3. The fourth curve relative to DB4, exhibiting values much lower than the three others, is not taken into consideration in averaging. It is well known that fibre reinforced materials often show an uneven distribution of the fibres regarding their orientation and their local volume concentration [8–13]. These irregularities are inherent to this kind of materials, consequently, such materials cannot be considered as purely homogenous. This unevenness affects less or more severely the mechanical properties of fibre reinforced materials. In a recent work related to the used UHPFRC in this contribution and published in [5,11,13,14], the variability of the mechanical and physical properties of specimens cut in different directions at different positions in an UHPFRC-panel, has been analysed by means of stereological principles. The results showed a wide scatter of the mechanical properties, whereas the physical properties, especially the air permeability, were only slightly subjected to scatter. For example, Fig. 2 shows a correlation between the tensile strength and the coefficient of fibre orientation [5].

Commercial ready mixed concrete (C30/37) with aggregate size of 16 mm is used to cast the RC elements. The average values of the concrete properties, based on standardized tests during the beam tests for concrete age between 126 and 246 days, are reported below in Table 1 [6]. Mean values of UHPFRC derived from curves of Fig. 1 are also given below in Tables 2 and 3.

The objective of the numerical simulation is to trace the experimental structural behaviour of a series of composite cantilever beams up to collapse conducted in an experimental program outlined in [6,7]. Once the numerical model is validated by experimental findings, it can be used with more safety and security for analysing large complex composite structures subjected to different loading conditions. The model is elaborated and analysed by means of the FEA software DIANA [1].

2. Brief description of experiments

Experimental procedure and results are briefly discussed in this paper. Full details can be found in [6,7]. In the sequel, a series of three cantilever beams with a total length of 2000 mm and a depth of 150 mm is analysed by means of non-linear FEA. The beam, denoted by MW0, is a monolithic RC beam with a height of 250 mm (after surface preparation and before casting the UHPFRC layer), serving as reference specimen for comparison with the UHPFRC/RC composite specimens. The structural capacity of the reference beam MW0 is increased by adding a layer of UHPFRC, i.e., beam strengthening is investigated. MW1 is a composite beam consisting of a RC beam with a thickness of 250 mm and covered

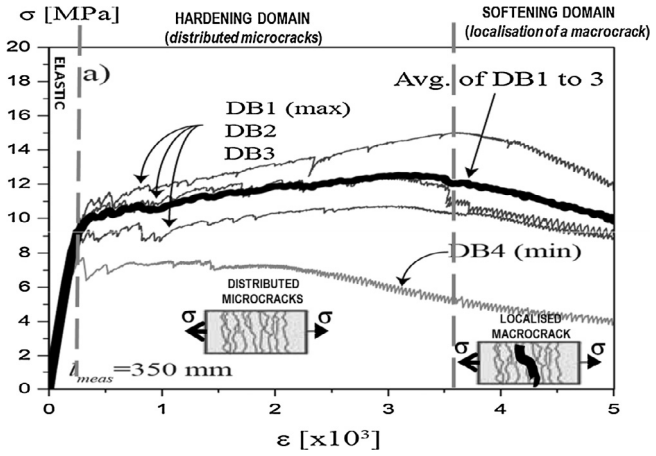

Fig. 1. Tensile behaviour of plain UHPFRC from cast dog-bone specimens with a length of 350 mm. Diagrams obtained for the four tested specimens, named DB1 to DB4, are given in gray; the mean curve is represented by the thick black curve [5].

on its top surface with a thin layer of UHFPRC with a thickness of 50 mm. Finally, the third specimen, denoted MW4, is a R-UHPFRC/RC composite beam identical to MW1, but the UHPFRC layer is reinforced longitudinally at its mid-depth by 4 equidistant steel rebars with a diameter of 8 mm. Steel reinforcement of the RC beams (substrate) of the composite beams MW1 and MW4 is identical to the reinforcement of the monolithic beam MW0. Fig. 3 gives in detail the geometry as well as the distribution and diameters of the steel reinforcement bars and stirrups for the three specimens.

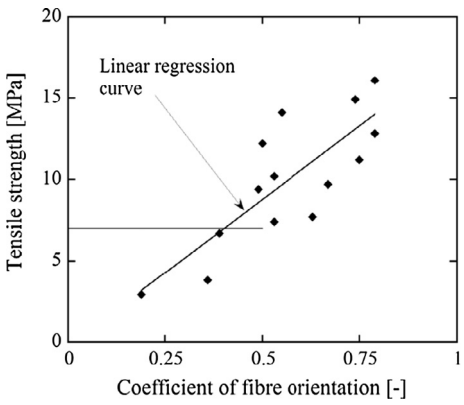

Fig. 2. Tensile strength of UHPFRC as function of the coefficient of fibre orientation [5].

Table 1
Tensile properties of concrete (linear and softening phases). **ε**: elastic strain, W: crack-opening and $G_{F,C}$, fracture energy.

Elastic Properties			Softening Properties, $G_{F,C}$ = 97 N/m		
E_c [kN/mm^2]	f_{Cte} [N/mm^2]	ε_{Cte} [0/00]	$f_{Cs,1}$ [N/mm^2]	$W_{Cs,1}$ [mm]	$W_{Cs,max}$ [mm]
29.90	3.80	0.131	0.95	0.021	0.12

Table 2
Tensile properties of plain UHPFRC (linear and hardening phases). **ε**: elastic and hardening strain.

Elastic properties			Hardening properties	
E_U [kN/mm^2]	f_{Ute} [N/mm^2]	ε_{Ute} [0/00]	f_{Utu} [N/mm^2]	ε_{Utu} [0/00]
42.00	8.50	0.21	12.00	2.50

Table 3
Tensile properties UHPFRC (softening phase). W: crack-opening and $G_{F,U:}$ fracture energy.

Softening properties, $G_{F,U}$ = 47.7 kN/m				
$f_{Uts,1}$ [N/mm^2]	$f_{Uts,2}$ [N/mm^2]	$W_{Uts,1}$ [mm]	$W_{Uts,2}$ [mm]	$W_{Uts,max}$ [mm]
6.00	2.50	3.25	6.40	10.50

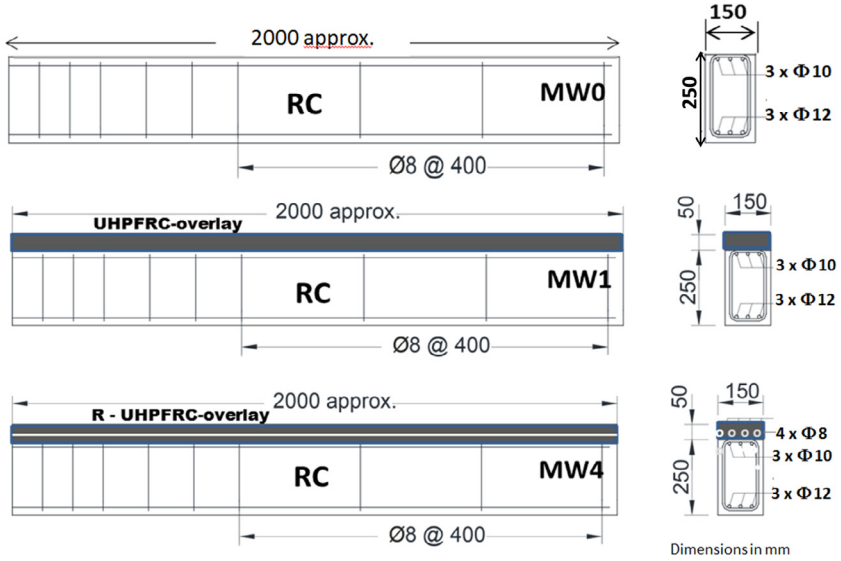

Fig. 3. Geometry and localization of the steel reinforcement bars of the three beams [6,7].

The experimental set-up is identical for all beams and is depicted in Fig. 4; values of geometrical parameters "a" and "l" are 800 and 1600 mm, respectively. As illustrated in the figure, the span between the pin and the roller is vertically prestressed by means of sandwich steel plates held together with a pair of threaded rods. This system ensures the fixity of the cantilever beam and increases the shear resistance of the beam part between the pin and the roller, thus preventing unwanted shear failure [6,7]. Specimens are subjected to quasi-static loading under actuator displacement control mode, by imposing a gradually increasing displacement at point D (Fig. 3) while recording the resisting force.

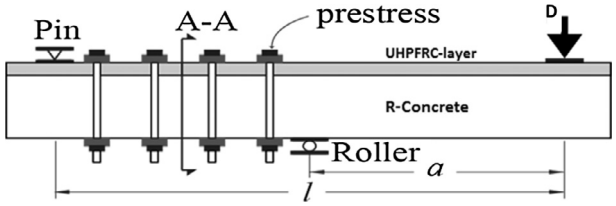

Fig. 4. Typical test setup of the cantilever beams [6,7].

3. Finite element mesh

FE-mesh and boundary conditions of a typical cantilever composite beam are depicted in Fig. 5. The element size varies: the region of main concern, namely the area between the roller and the concentrated force is slightly more refined compared to the rest of the specimen. Due to the absence of any symmetry, the full beam is modelled. A roller supports the beam vertically. A gradually increasing displacement is imposed at the central node of the steel plate (point "D" in Fig. 5) in the vertical direction. A pin is used at the point ("PIN" in the figure) situated symmetrically to the point-force ("D" in the figure), preventing an upward displacement. Concrete, UHPFRC and steel plates are modelled using quadrilateral plane stress elements.

4. Constitutive laws for concrete, UHPFRC and steel reinforcement

Since the 1980s, nonlinear finite element analysis has been proved to be a powerful tool to study, as realistically as possible,

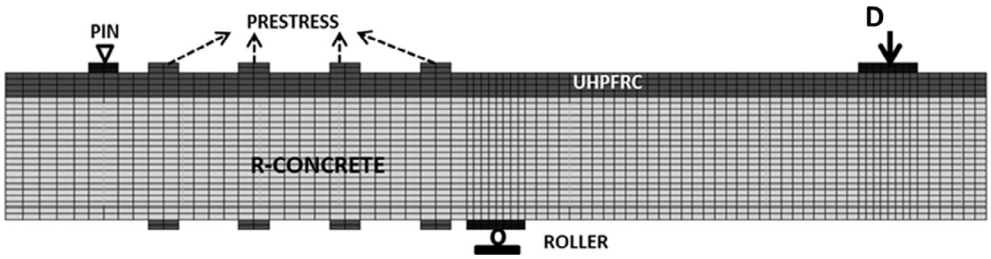

Fig. 5. FE-idealization of a typical UHPFRC – RC cantilever composite beam including the components of the loading setup and boundary conditions.

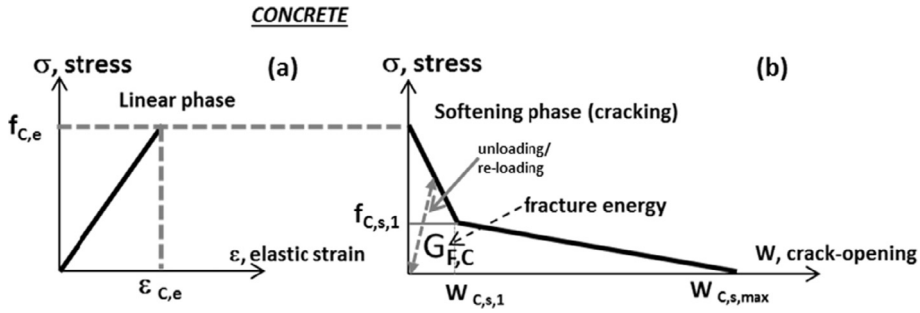

Fig. 6. Tensile laws for plain concrete consisting on two phases; linear phase (a) and softening phase (cracking) defined by a piecewise linear diagram (b).

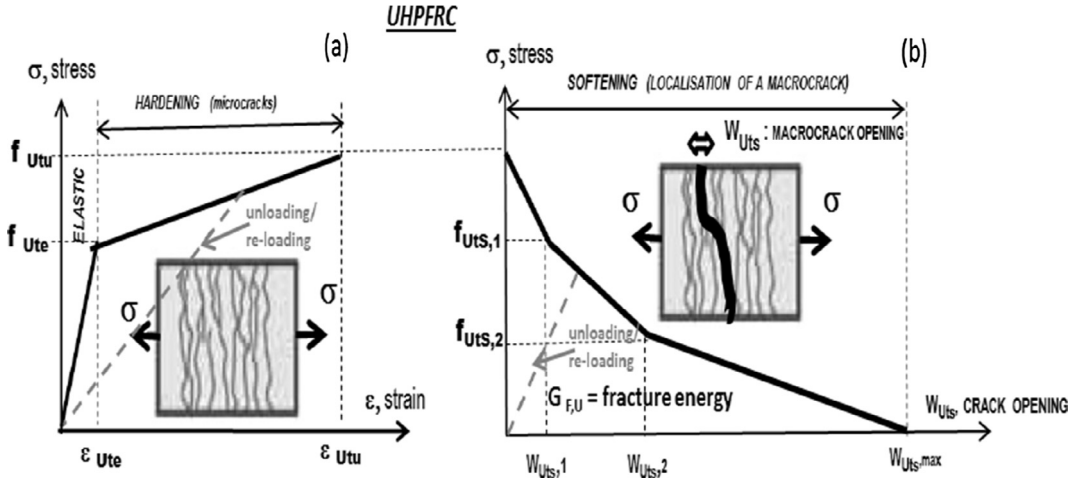

Fig. 7. Tensile laws for plain UHPFRC consisting on the elastic-hardening phase (a) and the softening phase defined by a piecewise linear diagram (b).

the behaviour of RC structures subjected to complex loading. Crack formation and propagation is undeniably the most important nonlinear phenomenon in concrete-like structures. Significant effort has been dedicated in the past years to develop fracture mechanics models based on realistic nonlinear material laws and to implement them in numerical FE-codes for predicting the mechanical behaviour of structures submitted to normal or even severe loading conditions.

Two different concepts are commonly used in FE-codes for computational simulation of crack propagation in RC structures, namely the discrete and smeared crack approaches [15–18]. The first concept, the Discrete Crack Approach, models a crack as a geometrical discontinuity. Such models are mainly used in structures in which the crack path is known beforehand; unfortunately, in most structures, crack paths are not known in advance. For the second concept, the Smeared Crack Approach, cracks are assumed to be smeared out over the continuum finite elements and a predefined position of cracks is not needed. A cracked material is then treated as a continuum, but with modified material properties to account for cracking. Smeared crack models allow for multiple cracking and propagate simultaneously on different and arbitrary locations in the structural member and with different orientations. In smeared crack models, in general, two concepts are often used to determine the crack evolution after its initiation, namely the rotating crack and the fixed crack concept. The total strain rotating crack model considers that the orientation of a crack co-rotates with the directions of the principal axes during the loading process, while for the fixed crack model, based on strain decomposition, the crack orientation remains fixed after its initiation during the loading process.

In this work, numerical modelling is carried out by means of the FE software DIANA [1], which has proved for decades, to be suc-

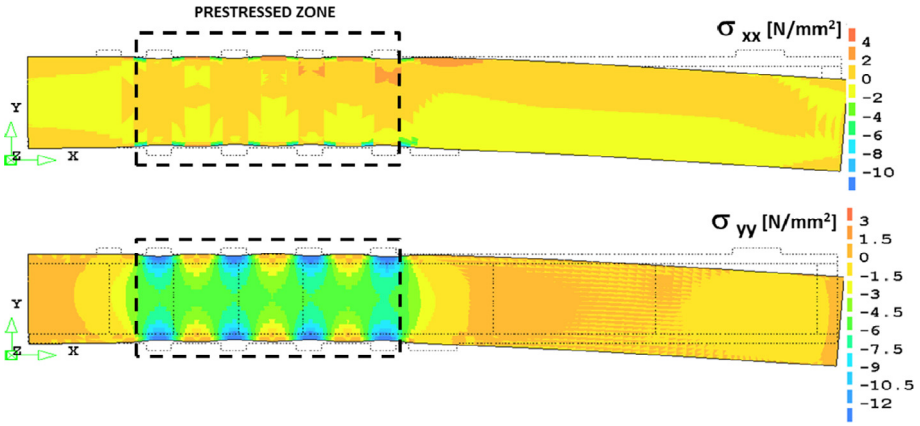

Fig. 8. Stress distribution and deformed shape of the cantilever beam MW0 at the end the linear regime (force level. 7.40 kN, just before start of softening).

cessful for analysing complex RC structures. In DIANA, smeared crack models in tension are used with orthotropic hardening and softening material behaviour. The cracked element is orthotropic with respect to the direction of the principal stress. The crack is smeared out over the continuum element. Both types of smeared cracks models, fixed and rotating, are available and described in detail in DIANA software [1].

According to many authors [19–23], rotating crack concept is more suitable and gives reasonably accurate results under monotonic load where principal stress slightly rotates during the loading process, for reinforced concrete structures. For that reason, the rotating crack model is used in this work to simulate the mechanical behaviour of tested cantilever composite beams subjected to monolithic load. The rotating crack model is based on the total strain, also called the "Total Strain Rotating Model", which describes the tensile and compressive behaviour of a material with one stress-strain relationship [24,25]. In DIANA, for tensile behaviour of the total strain crack model several predefined stress-strain functions are available.

A piecewise linear function type is employed for describing constitutive laws for both concrete and UHPFRC. Fig. 6 gives diagrams for the tensile laws for concrete, subdivided by the elastic phase (Fig. 6a) and the softening phase (Fig. 6b). Diagrams of the tensile parameters of the UHPFRC are depicted in Fig. 7a for the elastic and hardening phase and in Fig. 7b for the softening phase. In Figs. 6a and 7a, stresses are given as function of elastic (elastic-hardening for UHPFRC) strain; while in softening phase (Figs. 6b and 7b) tensile stresses are given as function of crack-opening (W). In the modelling, crack-opening are transformed into strain (strain softening) obtained by normalizing crack-opening (W) by the relevant crack bandwidth (h) defined below, in order to make results mesh size independent.

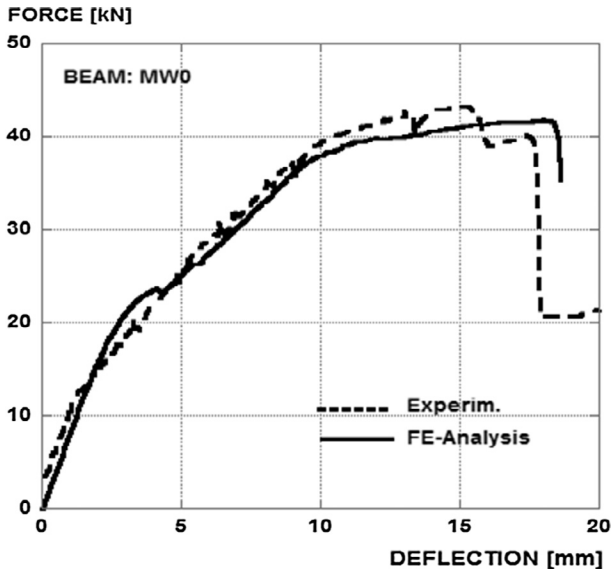

Fig. 9. Comparison between experimental force-deflection response of the monolithic RC cantilever beam MW0 (dashed curve) and the predicted one by the numerical model.

During the gradual loading process, due to stress redistribution, existing cracks can close and reopen in further load steps. In DIANA, closing and reopening of cracks are simply done by a secant modulus, meaning that the stress-strain relation goes linearly back to zero in the unloading phase, as shown in Fig. 6 which depicts an idealized piecewise linear function of the tensile stress-strain-softening relationships for concrete and stress-strain-hardening and stress-strain-softening for UHPFRC (Fig. 7a and b). The unloading and reloading assumption is a simplification, because in reality, many authors reported in their experimental findings, that there is a significant residual strain upon closing of a crack for examples [26,27] for concrete, and [28] for UHPFRC. Poisson's ratio is set to 0.2 for both materials and kept constant throughout the loading process.

The compressive behaviour of a total strain crack model is in general a nonlinear function between the stress and the strain. As in the case of tensile behaviour, DIANA [1] integrates several predefined non-linear functions for compression behaviour. In this sequel, an ideal elastoplastic curve is used for the compressive behaviour of both concrete and UHPFRC; curves are then simply characterized by Young's modulus and compressive strength of the materials. Compressive strengths are 28.0 and 115.0 N/mm^2 for concrete and UHPFRC, respectively.

The theoretical formulation of the model, the adopted numerical procedures and solution strategy adopted are described in details in DIANA user's manuals [1].

For smeared cracks, the fracture energy is distributed over a crack bandwidth (*h*), which is related to the particular finite element size and configuration. In that way, the fracture is released over this width of the FE in order to obtain results that are objective with regard to mesh refinement [16–18]. For 2D finite elements, the crack bandwidth *(h)* is set to the square root of the area of the cracked element *(A)*. This hypothesis gives a good compromise in terms of preserving results independent of the mesh refinement according to several authors.

Bars reinforcement have the shape of a line (1D elements) embedded in the surrounding finite elements (so-called mother

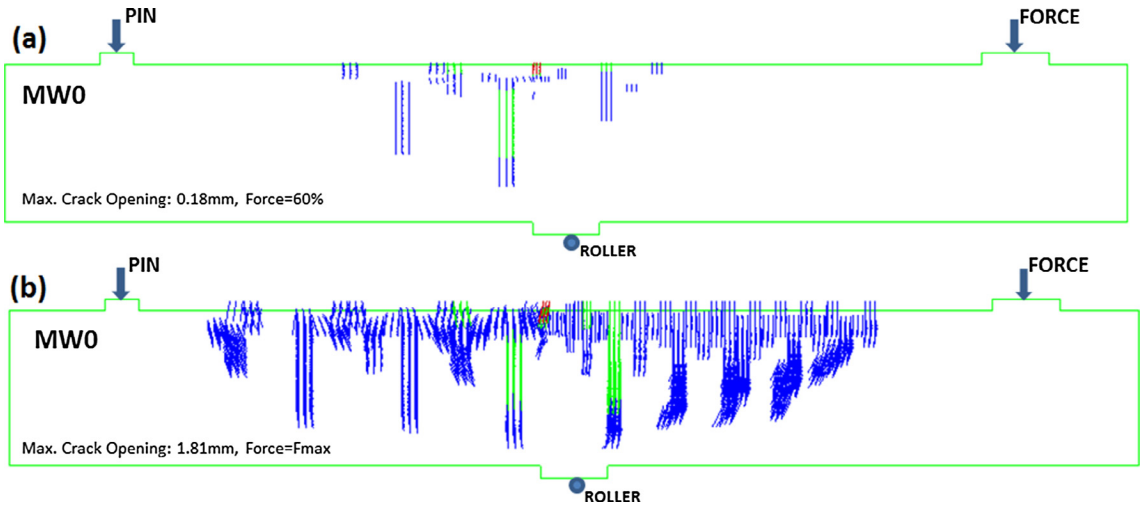

Fig. 10. Simulated cracking patterns of the monolithic cantilever beam MW0 at two force-levels. Red, green and blue colored bars correspond respectively to cracks with large, middle and small opening.

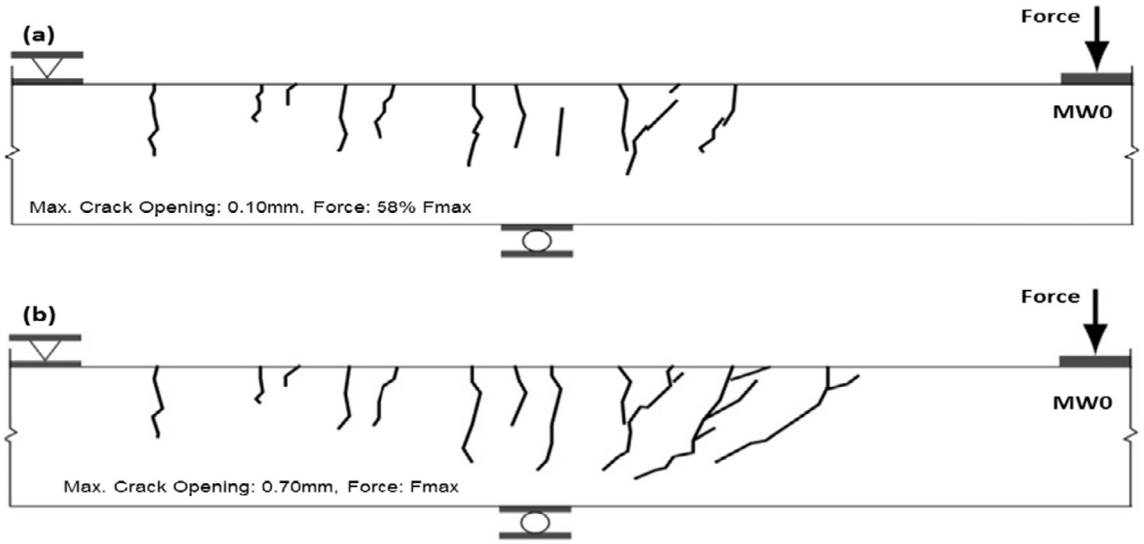

Fig. 11. Observed crack patterns (visible cracks) of the monolithic cantilever RC-beam MW0 at two force levels [6,9].

elements) of concrete (or UHPFRC). This modelling applies also for stirrups. An elastoplastic constitutive law with hardening models the mechanical behaviour of steel reinforcement bars and stirrups. Young's modulus of steel is set to 210 GPa, while the yield strength ranges from 500 to 600 MPa, depending on the diameter of rebars. Poisson's ratio is set to 0.3. In addition, a perfect bond is assumed between reinforcing bars and surrounding cementitious materials. Finally, all steel plates of the setup are assumed to behave in a linear elastic manner.

5. Numerical versus experimental results

This section presents numerical results and their confrontation with the corresponding experimental findings. Before selecting the appropriate solution procedures for solving the nonlinear problem, trials using different numerical strategies available in DIANA, are carried out. Performance of the tested procedures is assessed by comparing numerical results (force-deflection) with the corresponding experimental responses. On the basis of the conclusion of the preliminary analysis, the convergence criterion based on force norm with a tolerance set at 2.5% is adopted.

5.1. Monolithic cantilever beam, MW0

Fig. 8 shows stress distributions σ_{xx} and σ_{yy} and deformed shape of the cantilever beam (MW0) in the linear elastic regime (before onset of any crack, force: 7.40 kN). Fig. 9 gives a comparison between the simulated force-deflection response of the monolithic beam and the experimental curve.

We can observe a good agreement between the computed curve and the experimental one. The model predicts quasi-perfectly the force-deflection curve throughout the loading history. The computed peak-force (41.60 kN) is almost equal to the measured one (43.00 kN). Both experimental and predicted curves show a sudden drop of the force just after the peak-resistance and at roughly the same deflection level.

Fig. 10 shows predicted crack patterns of MW0 at a force level of 58% of $F_{max.}$ and at the peak-resistance ($F_{max.}$); cracks are represented by small bars located at gauss points in softening regime. For comparison purposes, Fig. 11 shows visible cracks recorded on one face of the monolithic beam MW0, at roughly the same force-levels as those selected in simulation (Fig. 10).

In the numerical model, at 60% of the peak-force (Fig. 10a), cracking consists, globally, on a series of vertical microcracked bands, starting from the upper layer of the beam and propagating further downwards. During the loading process, some existing cracks widen and propagate further, other close and simultaneously, new cracks initiate. At approximatively the peak-force, some of the cracked bands, located between the roller and the loading point, progress deeper towards the bot-

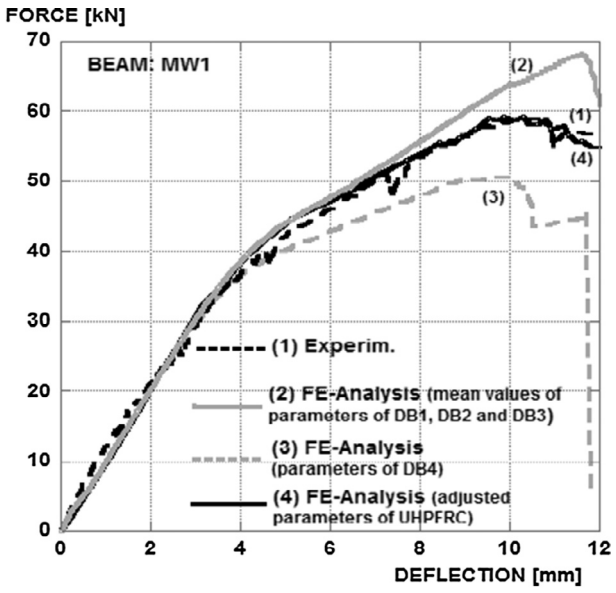

Fig. 12. Comparison between experimental force-deflection response of the RC/UHPFRC cantilever beam MW1 and the numerical results.

tom of the specimen. We can also notice in Fig. 10, that, even in the prestressed region (between the roller and the pin), scattered vertical cracked bands are formed; which is in accordance with the experimental observations (Fig. 11).

The computed maximal crack widths (Fig. 10) are larger than those recorded experimentally, nevertheless there are in the same order of magnitude. Comparing experimental crack patterns to the numerical ones, we can conclude that the model needs to be further improved in order to obtain a better concordance; especially the model do not shows clearly bifurcation of macrocracks downwards the roller as observed experimentally.

5.2. RC/UHPFRC composite cantilever beam, MW1

Fig. 12 shows a comparison between experimental and simulated force-deflection responses of the composite beam MW1. In the analysis of MW1 and MW4, using directly tensile parameters of UHPFRC (f_{Ute} and f_{Utu}) given in Table 3 lead to an overestimation of the force-deflection responses compared to experimental findings. Few attempts have been carried out by varying slightly f_{Ute} and f_{Utu} around mean values, in order to achieve a better agreement between experimental and computed force-deflection responses for both MW1 and MW4. It has been found that values of 8.0 and 10.5 N/mm^2 for f_{Ute} and f_{Utu}, respectively, gave an excellent deal for both composite beams. These "adjusted" values are lower than the mean values reported in Table 2; nevertheless they are reasonable due the experimental scatter as it can be seen in Fig. 1. Fig. 12 shows the comparison between the experimental structural response (black dashed curve (1)) and the simulated one with "adjusted" (thick black curve (4)). According to Fig. 1, the "adjusted" parameters are more representative of the curve relative to the dog-bone DB3. As it is depicted in Fig. 12 (curve (2)), the mean values (Table 3) overestimate the experimental response at elevated force-level. Material parameters resulting from DB4 clearly underestimate the experimental response shown in Fig. 12 (grey dashed, curve (3)). Finally, the force-deflection response, obtained with the "adjusted" parameters (curve (4) in Fig. 12), follows accurately the experimental curve throughout the loading process. The sudden drop of the force is predicted at about the same deflection level as in the test. The maximal computed force (F num. = 59.10 kN) is practically the same as the measured one (F exp. = 58.90kN).

In addition and in accordance with the experimental findings, the model predicts an increase of the peak-resistance of roughly 40% when the beam is strengthened by an UHPFRC layer comparatively to RC-monolithic beam (MW0). Both the increase in static height and the additional tensile capacity of the UHPFRC layer lead to this increase in bending resistance of the strengthened beam MW1.

A slight reduction in the deflection at maximum force of the strengthened beam MW1 is observed when compared with MW0. This may be explained by different ductility characteristics of the two materials: while the steel rebars with significant yield deformation are the only tensile reinforcement in MW0, the UHPFRC actually adds a lower deformation capacity to the strengthened system MW1.

Fig. 13 shows the predicted crack pattern of the MW1 composite beam at two selected force levels. Cracks are represented by small bars located at Gauss points. In the UHPFRC layer only cracks in the softening phase are shown (not those in the hardening domain). At roughly 85% of the peak-resistance (Fig. 13a), cracking consists on several vertical microcracked bands in concrete substrate, while no signs of any crack in the UHPFRC-layer. At the peak-force (Fig. 13b), the cracked bands in concrete substrate propagate further downwards the bottom, while only few cracks (softening domain) occur the UHPFRC-layer.

Fig. 14 displays the observed (visible) crack patterns at two force levels selected close to those chosen in the model (Fig. 13). Experimentally, cracking consists on few dispersed cracks converging obliquely downwards the roller. Unfortunately, the model does not reflect the same cartography of cracks as in the test, although maximal crack openings are roughly, in the same order of magnitude.

5.3. RC/R-UHPFRC cantilever composite beam MW4

Fig. 15 shows the comparison between the simulated and the experimental force-deflection responses of the composite RC/R-UHPFRC beam MW4. Material parameters are identical to those used in case of MW1. Once again, the model predicts excellently the experimental curve throughout the whole loading history.

The computed peak-resistance ($F_{num.}$ = 92.50 kN) is almost equal to the observed one ($F_{exp.}$ = 90.70 kN). The predicted maximum force occurs at approximatively the same deflection as in the test. Experimental and simulated curves show a sudden force reduction after the peak-resistance at roughly the same deflection. Both curves show an increase of the peak-resistance from 59 kN (MW1) to 90 kN when steel rebars are added to the UHPFRC-layer (MW4). The maximal force increases by 53% compared to MW1.

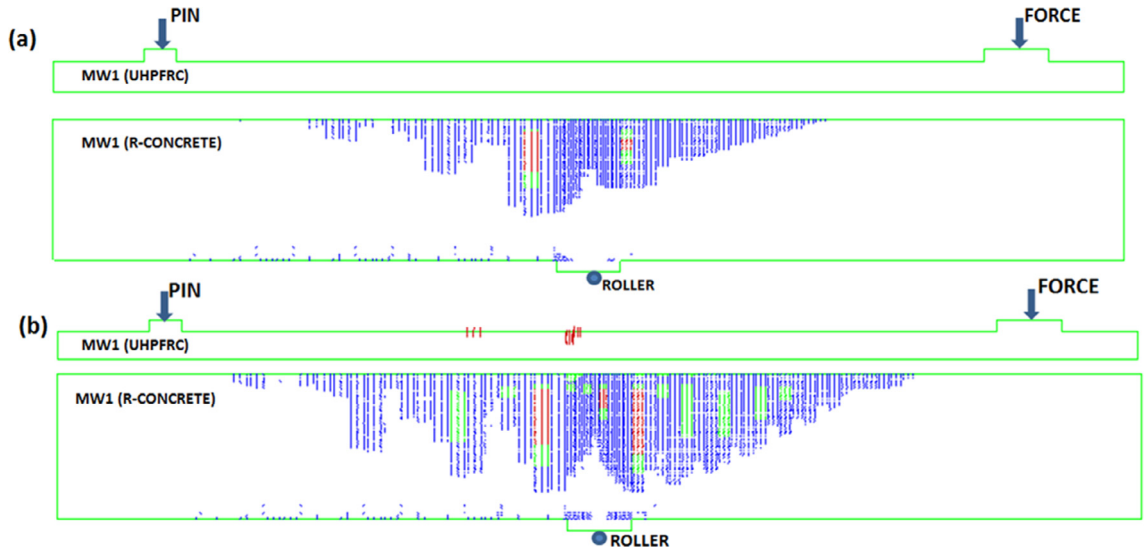

Fig. 13. Simulated cracking patterns of the RC/UHPFRC cantilever composite beam MW1 at two force levels. Red, green and blue colored bars correspond respectively to cracks with large, middle and small opening.

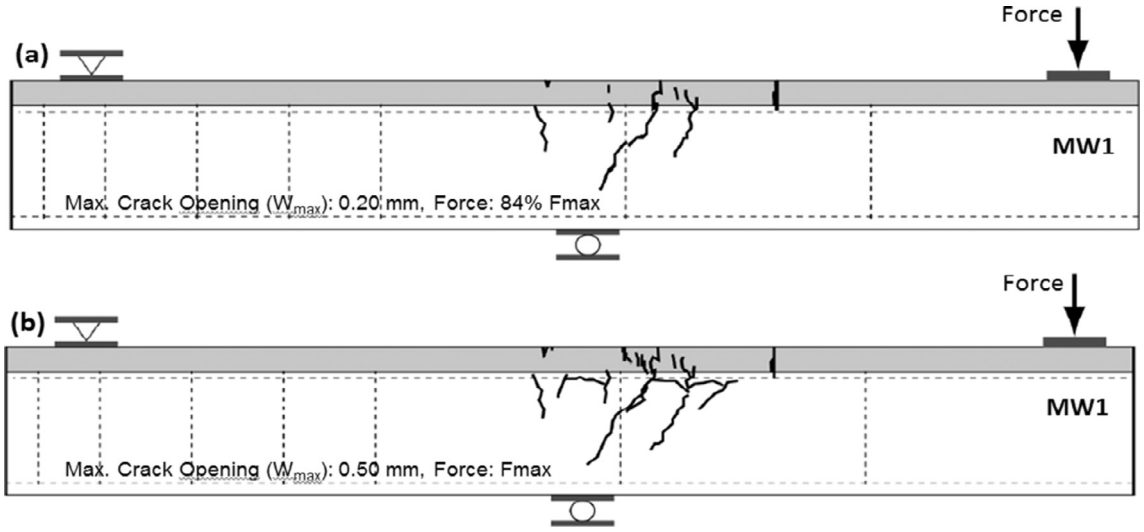

Fig. 14. Observed visible crack patterns of the composite cantilever RC/UHPFRC beam MW1 at two force-levels [6,9].

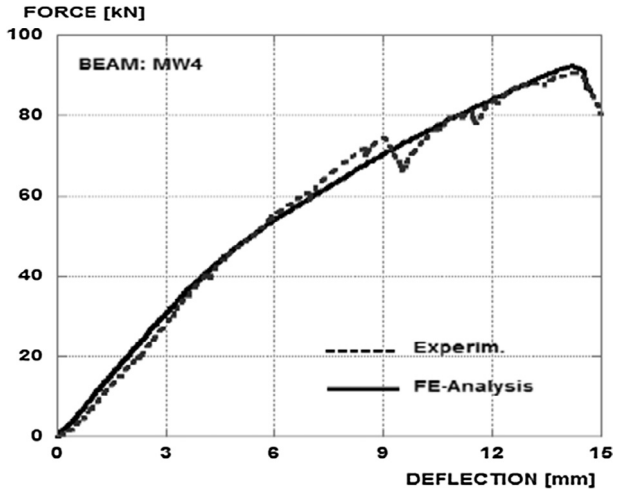

Fig. 15. Comparison between measured force-deflection responses of the RC/R-UHPFRC cantilever beam MW4 (dashed curve) and the predicted curve by the numerical model.

Fig. 16 displays the predicted crack patterns of the beam MW4 at two force levels. Cracks are represented by small bars located at Gauss points. The observed experimental (visible) cracks patterns are given in Fig. 17. We must acknowledge that simulated crack patterns do not faithfully reflect the experimental observation, although the structural response is accurately reproduced. This suggests that improvements must be made in modelling.

6. Conclusions

The structural behaviour of tested RC/R(UHPFRC) composite cantilever beams was simulated by a non-linear finite element analysis carried out with DIANA software. The model is based on the Smeared Crack Approach.

Excellent agreement is obtained between experimental force-deflection responses and the curves predicted by the numerical modelling. In particular, the peak-resistance is perfectly predicted.

In accordance with the experimental results, the UHPFRC layer increases considerably the resistance of RC beams (MW0) by roughly 40% (MW1). In addition, if the UHPFRC-layer is reinforced by steel rebars (MW4), the maximum force increases by 53% compared to MW1.

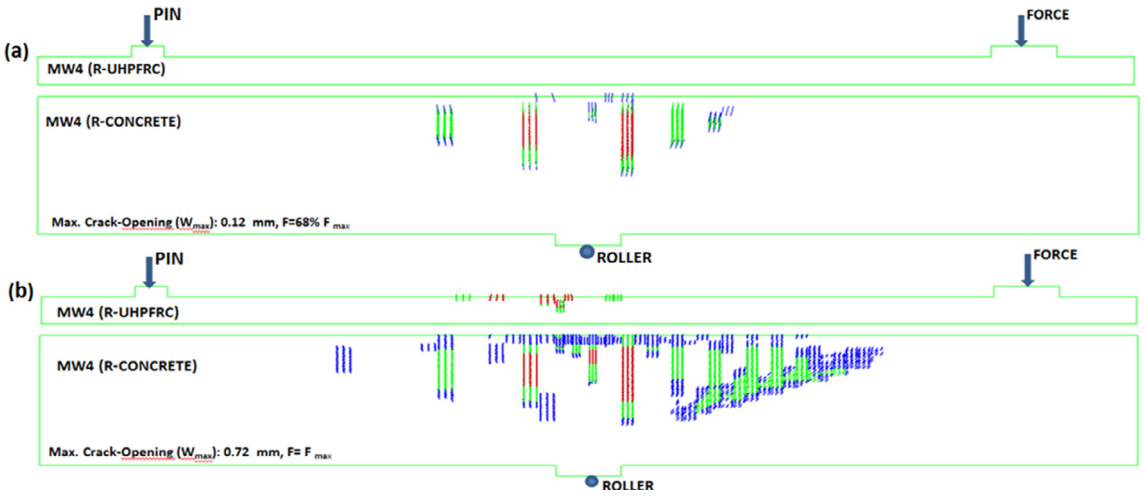

Fig. 16. Simulated cracking patterns of the RC/R-UHPFRC cantilever composite beam MW4 at two force levels. Red, green and blue colored bars correspond respectively to cracks with large, middle and small opening.

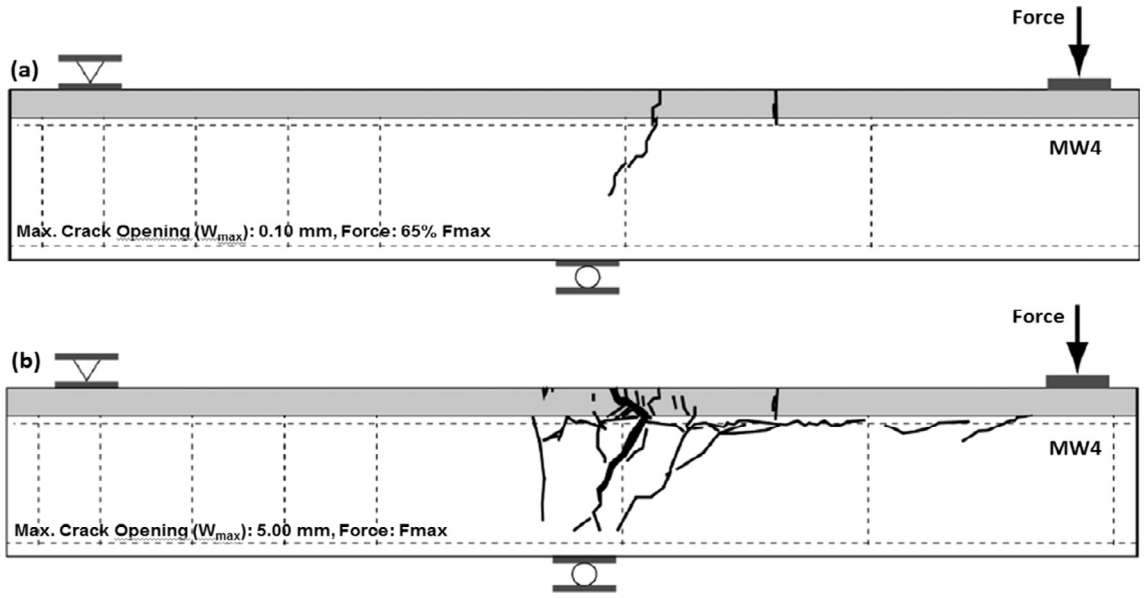

Fig. 17. Observed visible macro-crack patterns of the composite cantilever RC/R-UHPFRC beam MW4 at two force levels [6,9].

Concordance between experimental and computed crack patterns and crack openings is varying degrees of accuracy. The model must be further improved to reflect better experimental findings, especially regarding the crack patterns.

The numerical model can be further extended to explore the behaviour of real concrete structures (such as bridges) strengthened by a thin UHPFRC layer subjected to different loadings and environmental conditions like temperature variation, creep/relaxation, drying/autogenous shrinkage or ageing effects.

Formatting of funding sources

This research did not receive any specific grant from funding agencies in the public, commercial, or not-for-profit sectors.

References

[1] DIANA (Software), User's Manual, Release 9.4.4; TNO DIANA, The Netherlands, http://dianafea.com/fr, 2012.
[2] K. Habel, E. Denarié, E. Brühwiler, Experimental investigation of composite ultra-high-performance fibre reinforced concrete and conventional concrete members, ACI Struct. J. 104 (1) (2007) 93–101.
[3] J. Wuest, Comportement Structural des Bétons de Fibres Ultra Performants en Traction dans des Eléments Composés (Ph.D. thesis), EPFL Lausanne, Switzerland, 2007. no 3987.
[4] E. Brühwiler, E. Denarié, Rehabilitation of concrete structures using Ultra-High Performance Fibre Reinforced Concrete, in: proceedings of the Second International Symposium on Ultra High Performance Concrete, Kassel, Germany, (2008) 895–902.
[5] C. Oesterlee, Structural Response of Reinforced UHPFRC and Composite Members (Ph.D. thesis), EPFL Lausanne, Switzerland, 2010. n° 4848.
[6] T. Noshiravani, Structural Response of R-UHPFRC – RC Composite Members Subjected to Combined Bending and Shear (Doctoral thesis), École Polytechnique Fédérale de Lausanne, Lausanne, Switzerland, 2012.
[7] T. Noshiravani, E. Brühwiler, Experimental investigation on R-UHPFRC–RC composite beams subjected to combined bending and shear, ACI Struct. J. 110 (2) (2013) 251–261.
[8] L. Ferrara, A. Meda, Relationships between fibre distribution, workability and the mechanical properties of SFRC applied to precast roof elements, Mater. Struct. 39 (2006) 411–420.
[9] P. Stähli, R. Custer, J.G.M. van Mier, On flow properties, fibre distribution, fibre orientation and flexural behaviour of FRC, Mater. Struct. 41 (2008) 189–196.
[10] B. Boulekbache, M. Hamrat, M. Chemrouk, S. Amziane, Flowability of fibre-reinforced concrete and its effect on the mechanical properties of the material, Constr. Build. Mater. 24 (9) (2010) 1664–1671.
[11] C. Oesterlee, E. Denarié, E. Brühwiler, Strength and deformability distribution in UHPFRC panels. in: T. Uomoto, Proceedings CONMAT 09. Japan Society of Civil Engineers (JSCE), Japan Concrete Institute (JCI) and Canadian Society for Civil Engineering (CSCE), Nagoya, Japan, 2009, pp. 390–397.
[12] E.V. Sarmiento, M.A.N. Hendriks, M.R. Geiker, T. Kanstad, Modelling the influence of the fibre structure on the structural behaviour of flowable fibre-reinforced concrete, Eng. Struct. 124 (2016) 186–195.
[13] M. Bastien-Masse, E. Denarié, Brühwiler, Effect of fibre orientation on the in-plane tensile response of UHPFRC reinforcement layers, Cem. Concr. Compos. 67 (2016) (2016) 111–125.
[14] E. Denarié, E. Brühwiler, Strain-hardening ultra-high performance fibre reinforced concrete: deformability versus strength optimization, Restor. Build. Monum. 17 (6) (2011) 1–14.
[15] Y.R. Rashid, Analysis of Prestressed Concrete Pressure Vessels, Nucl. Eng.. Des. 4 (1968) 334–344.
[16] Z.P. Bazant, J. Planas, Fracture and Size Effect in Concrete and Other Quasibrittle Materials, CRC Press, Boca Raton, Florida and London, U.K., 1998.
[17] J.G. Rots, Comparative study of crack models, in: Hendriks & Rots (Eds.), Finite Element in Civil Engineering, 2002, pp 17–28.
[18] J.G. Rots, J. Blauwendraad, Crack models for concrete: discrete or smeared: fixed, multi-directional or rotating?, Heron 34 (1) (1989)
[19] R. Burgers, Nonlinear FEM modelling of steel fibre reinforced concrete. Report TU-Delft, 2006.
[20] K. Maekawa, A. Pimanmas, H. Okamura, Nonlinear Mechanics of Reinforced Concrete, Spon Press, 2003.
[21] Noon F. Silva Mamede, A. Pinho Ramos, Duarte M.V. Faria, Experimental and parametric 3D nonlinear finite element analysis on punching of flat slabs with orthogonal reinforcement, Eng. Struct. 48 (2013) 442–457.
[22] J. Nogueira, Numerical analysis of punching shear behavior of flat slabs strengthened with steel bolts (Master thesis), New University of Lisbon, Faculdade de Ciencias e Tecnologia, Monte da Caparica, 2011.
[23] A. Kupryciuk, S. Georgiev, Shear Distribution in Reinforced Concrete Bridge Deck Slabs, Department of Civil and Environmental Engineering. Division of Structural Engineering. Concrete Structures. Chalmers University of TechnologY Göteborg, Sweden 2013.
[24] R. de Borst, L.J. Sluys, Computational methods in non-linear solid mechanics. Report, TU-Delft, 2002.
[25] R. de Borst, P. Nauta, Non-orthogonal cracks in a smeared finite element model, Eng. Comp. 2 (1985) 35–46.
[26] H.W. Reinhardt, Fracture mechanics of an elastic softening material like concrete, Heron 29 (2) (1984) 1–42.
[27] H.W. Reinhardt, H.A.W. Cornelissen, D.A. Hordijk, Tensile test and failure analysis of concrete, J. Eng. Struct. 112 (11) (1986) 2462–2477.
[28] E. Denarié, Essais de caractérisation – réponse en traction. 2nd Workshop on " Béton Fibré Ultra-Performant", Haute Ecole d'Ingénieurs et d'Architecture Fribourg, Switzerland, 2015.